frontiers | Frontiers in Energy Research

ORIGINAL RESEARCH
published: 12 April 2022
doi: 10.3389/fenrg.2022.875654

Transient Stability Analysis and Control of Distributed Photovoltaic Generators in the DC Distribution Network

Hanghang He, Yanghong Xia, Wei Wei and Pengcheng Yang*

College of Electrical Engineering, Zhejiang University, Hangzhou, China

As dominant power sources, the safe and reliable operation of photovoltaic (PV) generators is crucial for the DC distribution network. This study analyzes the transient stability of PV generators under large disturbances and proposes a variable parameter control strategy to suppress the transient instability. First, the transient stability of the PV generators is analyzed using the proposed power–voltage evolution curve. It is found that the PV side easily suffers undervoltage faults during the transient process, which will cause instability of the system. Based on the revealed unstable mechanism, the variable parameter control is proposed to enhance the transient stability of PV generators. Finally, all the findings have been validated by hardware-in-loop tests.

Keywords: DC distribution network, photovoltaic generators, transient stability, variable parameter control, power–voltage evolution curve

OPEN ACCESS

Edited by:
Ariya Sangwongwanich,
Aalborg University, Denmark

Reviewed by:
Rui Wang,
Northeastern University, China
Minghao Wang,
Hong Kong Polytechnic University,
Hong Kong SAR, China

****Correspondence:***
Yanghong Xia
royxiayh@zju.edu.cn

Specialty section:
This article was submitted to Solar Energy, a section of the journal Frontiers in Energy Research

Received: *14 February 2022*
Accepted: *14 March 2022*
Published: *12 April 2022*

Citation:
He H, Xia Y, Wei W and Yang P (2022) Transient Stability Analysis and Control of Distributed Photovoltaic Generators in the DC Distribution Network. Front. Energy Res. 10:875654. doi: 10.3389/fenrg.2022.875654

INTRODUCTION

In recent years, the demand for clean renewable energy sources has attracted the worldwide attention in order to alleviate the environmental degradation and the traditional fossil fuel energy depletion crisis (Chaiyatham and Ngamroo, 2017). As one of the most important renewable energy sources, solar energy is of great significance to energy security (Zhao et al., 2019), and photovoltaic (PV) power generation is the major form to utilize solar energy. Thanks to the technological advancements in solar cell manufacturing and semiconductors, the inexhaustible PV generators have been developed into one of the most prospective sources (Farsi and Liu, 2020) (Safayatullah et al., 2021).

PV generation technology has been developing rapidly all over the world; many scholars have conducted extensive and in-depth research on current issues such as PV system modeling (Li et al., 2011; Liu et al., 2011; Li, 2013), power generation (Eftekharnejad et al., 2015; Sangwongwanich et al., 2016; Fathabadi, 2019), materials (Uprety et al., 2018;Bosco et al., 2020), and control strategies (Shadmand et al., 2014; Weckx et al., 2014; Quan et al., 2020), and many achievements have been obtained. However, with the expansion of the PV power generation scale, especially as the role of PV power generation changes from auxiliary power to dominant power, its dynamic characteristics play an important role in the stable operation of power system. Due to the intermittent and fluctuation characteristics of PV power generation, its large-scale grid connection brings great challenges to the stability of the power system (Kawabe and Tanaka, 2015) (Wang et al., 2016).

PV generators show DC characteristics, and if they can be connected to the DC distribution, additional DC/AC conversion stages will be saved compared to being connected to the traditional AC distribution network (Azeem et al., 2020). On the other hand, the DC distribution network can also avoid additional DC/AC conversion stages when providing power for DC loads. Therefore, the

development of the DC distribution network can obviously improve system efficiency when the power system integrates DC sources and DC loads (Song et al., 2013). Nevertheless, with the high penetration of PV generators, the dynamics and characteristics of DC distribution network will be changed profoundly, and the system stability is greatly influenced (Eftekharnejad et al., 2013; Lammert et al., 2019).

Shah et al. (2015) extensively reviewed the stability challenges for the integration of large-scale PV generators. The existing studies on the stability analysis of PV generators can be divided into small-signal stability (Majumder, 2013; Coelho et al., 1999) and transient stability (or large-signal stability) (Ishchenko et al., 2006; Chen et al., 2010; Xiao and Fang, 2010; Fu et al., 2014). The former topic focuses on the system dynamics under small disturbances, while the latter topic mainly pays attention to the system dynamics under large disturbances. Much attention is paid to small-signal stability, and relevant research on different problems such as power harmonic stability (Wang and Blaabjerg, 2019; Wang et al., 2014), harmonic resonance (Hong et al., 2019; He et al., 2013), and weak grid (Xia et al., 2019; Dahal et al., 2011) are mature. Moreover, related analysis methods such as impedance analysis (Sun, 2011; Zeng et al., 2011; Zhou et al., 2018), modal analysis (Kouki et al., 2020), and state space method (Davari and Mohamed, 2017; Huang et al., 2015) have been discussed in depth. However, if large disturbances occur, the small-signal stability analysis is no longer applicable, and the transient stability analysis is indispensable. Transient stability refers to the ability of the system to resume normal operation after a sudden and serious failure occurs (Kundur, 1994), while only a few research studies can be found on this field, especially for the PV generators in the DC distribution network.

In Yagami and Tamura (2012), the influence of PV generators on transient stability of the power system has been analyzed using a single-machine infinite bus system. Furthermore, Liu et al. (2011) revealed the key factors that influence the transient stability including fault locations, disturbance types, topologies, and high PV penetration levels. In Priyamvada and Das (2020), a transient stability criterion for PV generators with DC-link control and reactive power control is proposed, and this criterion is applicable to all kinds of short circuit faults. Huang et al. (2019) explained the transient stability behavior of the droop-controlled voltage source converters (VSC) theoretically. This study shows that transient instability will occur to the droop-controlled VSC when its current is saturated under large disturbances. Then, a modified P-f droop control is proposed to deal with this problem and to enhance the system transient stability. In Zhang et al. (2017), the transient stability of the grid-connected VSC is analyzed by the modified equal area criterion. However, the conventional equal area criterion-based stability analysis is not applicable for PV generators connected to the DC distribution network.

The aforementioned research studies on transient stability analysis mainly focus on the AC distribution network which mainly draw lessons from the stability analysis of synchronous generators. Based on the power–angle relationships, the transient stability of PV generators connected to the AC distribution network can be analyzed effectively. Nevertheless, for the DC distribution network, there is no mature experience that can be referred to; hence, much fundamental research should be developed.

Wang et al. (2013) proposed a voltage hierarchical coordination control strategy. The operating state is switched in real time according to the DC bus voltage deviation value, which can maintain the system stability. However, it is difficult to give a good support if a sudden change occurs in DC bus voltage. Many scholars (Griffo and Jiabin Wang, 2012) (Jiang et al., 2019) constructed corresponding Lyapunov functions in order to analyze the convergence of the system trajectory and to determine the attraction domain of the system. Griffo and Jiabin Wang (2012) employed Brayton–Moser mixed potential functions to confirm the transient stability boundary of the whole system. Kabalan et al. (2017) reviewed the Lyapunov-based large-signal stability studies and proposed the direction for future research. In Jiang et al. (2019), an improved analysis method for transient response characteristics of the load converter is proposed, and a more precise stability criterion is obtained. However, the results of the Lyapunov direct method tend to be conservative, and there does not exist a widely accepted theory on how to construct Lyapunov functions. Compared with the full-fledged linear system analysis method, the information obtained from the Lyapunov function is very limited, which is not conducive to revealing the essential stability mechanism.

Focusing on the aforementioned challenges, this article proposes a new paradigm to analyze the transient stability of PV generators under large disturbances when they are connected to the DC distribution network. First, the large-signal model of a single-PV generator connected to the DC bus is established. Then, the transient stability of the PV generator during the DC bus voltage sag and recovery stages is analyzed using the proposed power–voltage evolution curve, which contrasts with the power–angle curve in the AC power system. The influence of corresponding control parameters is carefully studied, and the unstable mechanism is revealed. It is found that the PV side easily suffers undervoltage faults during the transient process, which will cause instability of the system. Next, the variable parameter control is proposed to enhance the transient stability based on the revealed unstable mechanism. The effectiveness of the proposed transient stability analysis and control methods is validated through related hardware-in-loop tests.

The remainder of this article is organized as follows: In *Large-Signal Model of PV Generators Connected to DC Distribution Network* section, the large-signal model of a single PV generator connected to the DC bus is established. Then, *Transient Stability Analysis Based on the Power–Voltage Evolution Curve* section analyzes the transient stability using the power–voltage evolution curve in detail. After that, the proposed variable parameter control method is introduced in *Variable Parameter Control for the Transient Stability Enhancement* section. The related real-time hardware-in-loop (HIL) tests are conducted in *Hardware-in-loop Tests* section. At last, *Conclusion* section concludes this article.

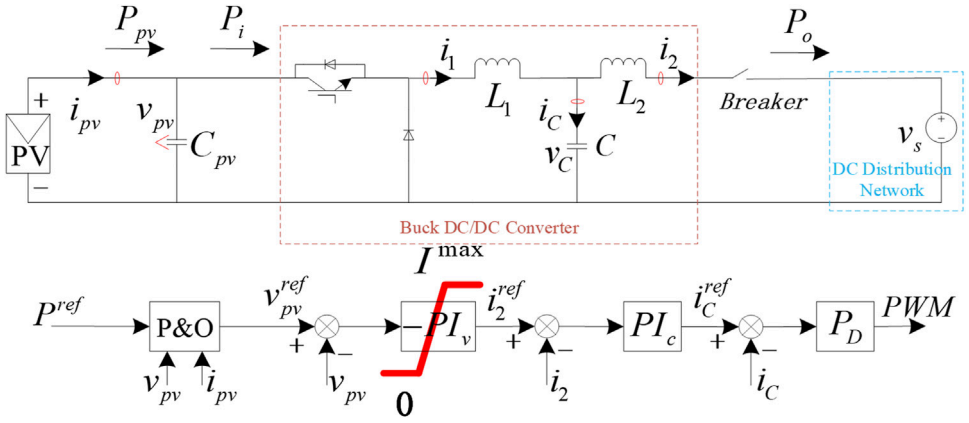

FIGURE 1 | Topology and control of a PV generator connected to the DC distribution network.

LARGE-SIGNAL MODEL OF PV GENERATORS CONNECTED TO THE DC DISTRIBUTION NETWORK

The topology of a PV generator connected to the DC distribution network is shown in **Figure 1**. The buck DC/DC converter is connected the PV generator and the DC distribution network. The capacitor on the PV side is C_{pv}; the output voltage, current, and power of the PV panel are v_{pv}, i_{pv}, and P_{pv}, respectively. The output of the buck DC/DC converter is filtered using an LCL filter, the corresponding inductors and capacitor are L_1, L_2, and C, whose inductive currents and capacitive voltage are i_1, i_2, and v_C. The input power and output power of the whole DC/DC converter system are P_i and P_o. The DC distribution network is simplified as an ideal voltage source v_s.

There is a breaker between the PV generator and the DC distribution network. If serious faults occur, the breaker will be triggered and the PV generator will be disconnected, especially when the input voltage of the buck DC/DC converter is lower than its output voltage, that is, $v_{pv} < v_s$.

Figure 1 also shows the control method, which is a typical multi-loop control strategy (Tafti et al., 2018). The whole control strategy can be divided into three parts, namely, the outermost loop, the middle loop, and the innermost loop. The outermost loop is a PV power control loop based on the perturbation and observation (P&O) method, which generates reference PV voltage v_{pv}^{ref} for the middle loop. The middle loop is the PV voltage control loop, which enables v_{pv} to follow the reference value v_{pv}^{ref} precisely through a proportional–integral (PI) controller. It is worth noting that this PI controller sets a limit I^{max} on the output amplitude to avoid overcurrent faults of the converter. At the same time, the middle loop generates the reference output current i_2^{ref} for the innermost loop. Last, the innermost loop is the output current control loop, which realizes accurate current tracking based on a PI controller. In addition, the proportional controller-based damping control is adopted to enhance the system stability.

Usually, the bandwidth of the innermost current loop is 10 times larger than that of the outer loop, as shown in **Figure 1**. Therefore, the system dynamics during large disturbances are mainly dominated by the slow outer loops. To simplify the analysis, the current loop can be viewed as a unity gain (Wu and Wang, 2020), and the output inductor current i_2 can track its reference value i_2^{ref} in time. Hence, it can be obtained as follows:

$$\begin{cases} \dfrac{di_k}{dt} = k_i\left(v_{pv} - v_{pv}^{ref}\right) \\ i_2^{ref} = k_p\left(v_{pv} - v_{pv}^{ref}\right) + i_k \\ i_2 = \begin{cases} i_2^{ref}, 0 \le i_2^{ref} \le I^{max} \\ 0, i_2^{ref} < 0 \\ I^{max}, i_2^{ref} > I^{max} \end{cases} \end{cases}, \tag{1}$$

where k_p and k_i are the proportional and integral coefficients of the PV voltage loop, i_k is the output of the integral controller, and I^{max} is the allowable maximum output current of the voltage control loop, as shown in **Figure 1**. Under large disturbances, the outermost power control loop will freeze its output v_{pv}^{ref} to avoid the disorder of the P&O method. Hence, v_{pv}^{ref} is constant during the large disturbance period. It can be seen that i_2 is greatly influenced by v_{pv}.

Furthermore, if the loss of the switch tubes and filters is ignored (Severino and Strunz, 2019), that is,

$$P_i = P_o = v_s \cdot i_2. \tag{2}$$

Then, the PV side model can be established as follows:

$$\begin{cases} \dfrac{1}{2} C_{pv} \dfrac{dv_{pv}^2}{dt} = P_{pv} - P_o \\ P_{pv} = v_{pv} \cdot N_p \left(I_{sc} + K_I \Delta T\right)\left[\dfrac{G}{G_N} - \dfrac{exp\left(v_{pv}/N_S V_t a\right) - 1}{exp\left(\left(V_{oc} + K_V \Delta T\right)/V_t a\right) - 1}\right] \end{cases}, \tag{3}$$

where N_p and N_S are the number of modules in parallel and series, respectively; I_{sc} and V_{oc} are short circuit current and open circuit voltage of a single module, respectively; K_I and K_V are the coefficients of current and voltage, respectively; ΔT is the

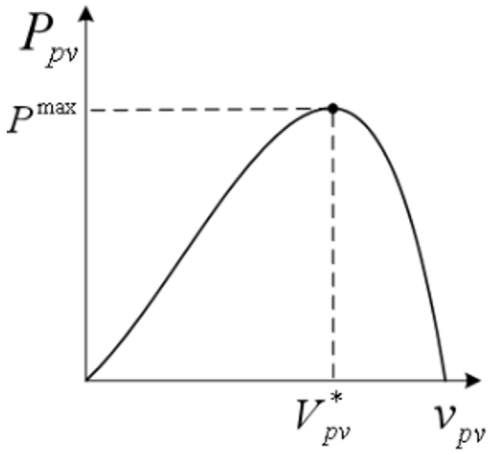

FIGURE 2 | Output model of a PV generator.

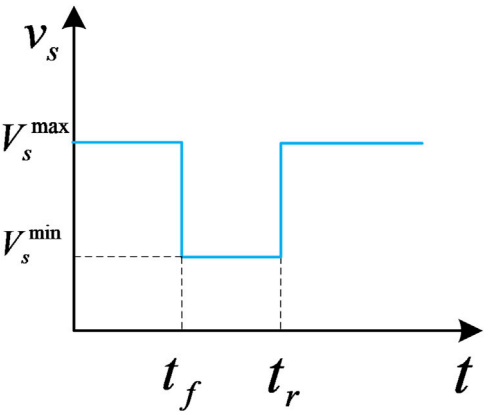

FIGURE 4 | Variation process of DC source voltage.

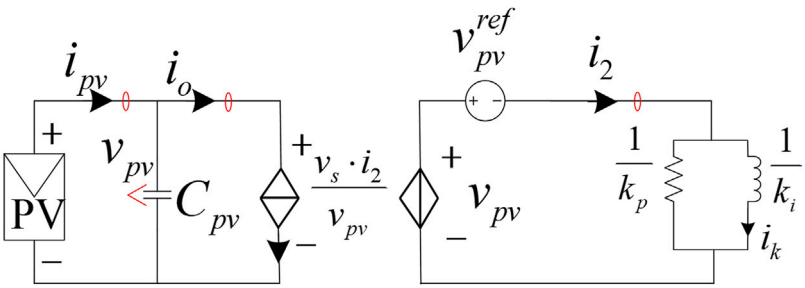

FIGURE 3 | Equivalent topology when analyzing the transient stability.

difference between the actual and rated temperature; G and G_N are the actual and rated irradiance, respectively; V_t is the thermal voltage; a is the ideal diode constant (Cai et al., 2018) (Villalva et al., 2009); and P_{pv} is the output power of the PV panels. The relationship between P_{pv} and v_{pv} is shown in **Figure 2**, where P^{max} is the maximum power and V_{pv}^{*} is the corresponding voltage.

Combining (1)–(3), the simplified large-signal model of the PV generator can be derived as shown in **Figure 3**. The PI controller of the PV voltage loop is equivalent to a parallel form consisting of a resistor and an inductor. The corresponding resistance and inductance are $1/k_p$ and $1/k_i$, respectively. It should be noted that the amplitude-limiting part of this PI controller are not presented, but its function is taken into consideration when the stability is analyzed. From this figure, it can be seen that the large disturbance of v_s can directly influence the PV side voltage v_{pv}, which makes v_{pv} exceed its normal range easily and causes the instability of the PV generator. In addition, the whole model is strongly nonlinear, including PV panels, power coupling, and amplitude limiting. Therefore, its transient stability analysis is challenging and needs new methods.

TRANSIENT STABILITY ANALYSIS BASED ON THE POWER–VOLTAGE EVOLUTION CURVE

In this section, the transient stability of the PV generator is analyzed when it suffers the DC bus voltage sag faults of the outer DC distribution network based on the established large-signal model in *Large-Signal Model of PV Generators Connected to DC Distribution Network* Section.

Figure 4 shows the typical DC bus voltage profile when sag faults occur. The voltage sag occurs at the time t_f and disappears at t_r. In this figure, V_s^{max} and V_s^{min} denote the DC bus voltage under the normal and fault states, respectively.

For the traditional AC distribution network, it is required that PV generators output maximum reactive currents to support the AC bus voltage. Hence, the PV side voltage is not tightly related to the AC bus voltage. However, for the DC distribution network, only the active power is considered and PV generators should output maximum active currents to support the DC bus voltage, and the active power will influence the dynamics of the PV side voltage. Therefore, the PV side voltage is tightly related to the DC bus voltage, as shown in **Figure 3**. This is the nature difference

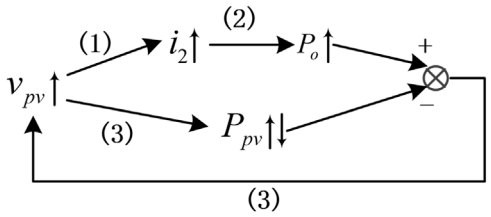

FIGURE 5 | Logical relation diagram of changes about P_o, P_{pv}, and v_{pv}.

between DC grid-connected PV generators and AC grid-connected PV generators.

When the DC bus voltage sag occurs, the original active power balance on both sides of the capacitor C_{pv} will be broken, which will change the charging and discharging states of C_{pv}. As a result, the value of PV side voltage v_{pv} will alter, which will affect the stability of the whole system.

From **Eqs 2**, **3**, it can be seen that the output power P_o and PV side power P_{pv}, are closely related to v_{pv} as shown in **Figure 5**. For example, when v_{pv} increases, i_2 will also increase according to the PI control relationship, as shown in **Eq. 1**, and then P_o will increase according to **Eq. 2**. Moreover, depending on the PV output model in **Figure 2**, P_{pv} may increase or decrease. When P_{pv} and P_o are not equal, capacitor C_{pv} will be in a charging or discharging state, further changing the value of v_{pv}. For the same analysis logic, a decrease in v_{pv} can be deduced. Hence, it is a good choice to describe the relationship between v_{pv} and P_o and P_{pv} using the power–voltage evolution curve as shown later.

Transient Process Under DC Bus Voltage Sag

In the analysis of this study, when the DC distribution network encounters a large disturbance, the transient evolution process can be divided into two stages, namely, the voltage sag stage and the voltage recovery stage of the DC bus. The whole system transient dynamics during the voltage sag and the recovery process using the power–voltage evolution curve are illustrated in **Figure 6**. The black curve describes the changing process of P_{pv} with v_{pv}, the red curve describes the correspondence between output active power P_o and v_{pv} during the voltage sag stage, while the blue curve represents the relationship during the voltage recovery stage. The arrows on each curve represent the movement path of the working point.

In the normal state, the PV panel tracks the maximum power point, that is, works at point 1 in **Figure 6**. In this state,

$$\begin{cases} \boldsymbol{P_{pv} = P_o = P^{max}} \\ \boldsymbol{v_{pv}^{ref} = V_{pv}^*} \end{cases}, \tag{4}$$

where P^{max} is the maximum power of the PV panel and V_{pv}^* is the corresponding maximum power point voltage.

When the DC distribution network suddenly suffers large disturbances, v_s drops sharply from V_s^{max} to V_s^{min} and P_o suddenly decreases too, that is, the operating point of P_o decreases from point 1 to point 2 instantly at the fault-occurring instant. Since PV power P_{pv} cannot change immediately, during this period, $P_{pv} > P_o$, the capacitor C_{pv} is in the charging state, the value of v_{pv} increases, and the operating point of P_{pv} moves from point 1 to point 4 on the black curve. As a result, the value of P_{pv} keeps decreasing.

According to (1), when v_{pv} increases, at first, i_2 keeps increasing until it reaches I^{max} and stays unchanged, and then P_o increases from point 2 to point 3, where $P_o = V_s^{min} I^{max}$. Later, P_o remains constant and the operation point moves from point 3 to point 4.

On the other hand, an increase in v_{pv} will lead to a decrease in P_{pv} when $v_{pv} > V_{pv}^*$. Finally, the operation point of P_{pv} moves to point 4, where P_{pv} is equal to P_o. At this point, the capacitor C_{pv} stops charging and v_{pv} reaches its maximum value V_{pv}^{max} and no longer increases, indicating that the system reaches the steady state.

After the DC bus voltage sag lasts for a period of time, the fault is cleared and the DC bus voltage returns to normal. The voltage recovery stage can be subdivided into three substages. Concretely, substage Ⅰ: v_{pv} decreases from V_{pv}^{max} to V_{pv}^*, substage Ⅱ: v_{pv} decreases from V_{pv}^* to V_{pv}^{min}, and substage Ⅲ: v_{pv} returns from V_{pv}^{min} to V_{pv}^*.

In substage Ⅰ, the fault disappears and V_s^{min} returns to V_s^{max} with a sharp rise. Then, P_o suddenly increases to the maximum value $P_o = V_s^{max} I^{max}$, and the operation point moves from point 4 to point 5.

During this period, $P_o > P_{pv}$, capacitor C_{pv} is in the discharging state, the value of v_{pv} decreases, and the operating point of P_{pv} moves from point 4 to point 1 on the black curve. As a result, the value of P_{pv} keeps increasing until v_{pv} is equal to V_{pv}^*.

Since v_{pv} is always larger than V_{pv}^*, i_2 stays the same as I^{max} because of the amplitude limiting part of the PI controller. P_o also

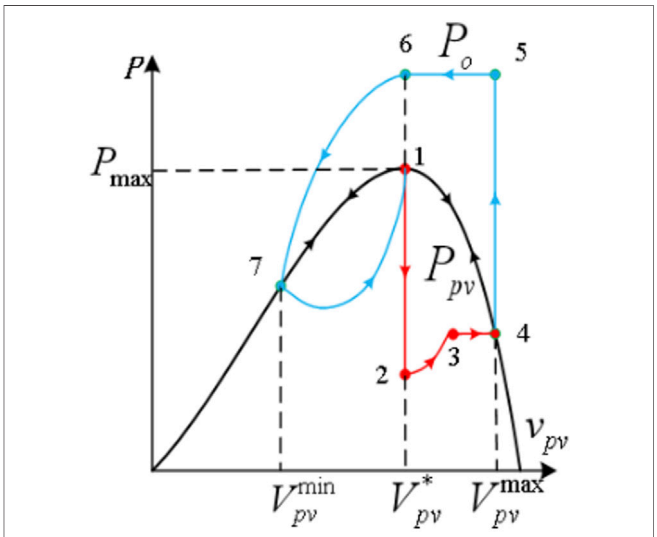

FIGURE 6 | Power–voltage evolution curve of the PV generator and the DC distribution network during the transient voltage sag and the recovery process.

stays unchanged, and the operation point moves from point 5 to point 6.

In substage II, v_{pv} continues to decline since $P_o > P_{pv}$. Then, $v_{pv} < V_{pv}^*$, causing the PI controller of voltage control loop to desaturate. The relationship between i_2 and v_{pv} can be rewritten as follows:

$$i_2 = I^{max} - k_p\left(V_{pv}^* - v_{pv}\right) - \int_{t_2}^{t} k_i\left(V_{pv}^* - v_{pv}\right)dt, \tag{5}$$

where t_2 denotes the time when v_{pv} decreases to V_{pv}^*. As v_{pv} continues to decline, both i_2 and P_o will decrease. In this substage, $P_o > P_{pv}$ all the time, so C_{pv} stays in the discharging state and v_{pv} keeps decreasing, and then P_{pv} will decrease until v_{pv} reaches V_{pv}^{min}, where P_{pv} is equal to P_o. We can see from **Figure 6** intuitively that the operation point of P_{pv} moves from point 1 to point 7 and P_o moves from point 6 to point 7. Then, v_{pv} reaches its minimum value V_{pv}^{min} and no longer decreases.

However, the system does not reach the steady state because the value of v_{pv} is not equal to V_{pv}^* and the output of the PI controller i_2^{ref} is still changing. Hence, in substage III, i_2 and P_o will decrease at first, then $P_o < P_{pv}$ indicating that the capacitor C_{pv} is in the charging state, so v_{pv} will keep increasing until V_{pv}^*. As a result, the operation points of P_o and P_{pv} retrace through the blue curve and black curve, respectively, and finally reach point 1 after several cycles of oscillation, and the system realizes stabilization. The whole dynamic process has been analyzed in detail using the proposed power–voltage evolution curve.

Influence of Parameters During the Voltage Recovery Stage

Following the analysis of the transient dynamic process during and after voltage sag, the influence of parameters is analyzed in this section.

First, from the perspective of small-signal stability, the bandwidth of voltage loop and current loop should be matched with each other. If the control parameters k_p and k_i are too large, the bandwidth of the voltage loop is close to or even exceeds the bandwidth of the current loop, which will jeopardize the small-signal stability of the whole system.

Furthermore, as mentioned in *Large-Signal Model of PV Generators Connected to DC Distribution Network* section, the buck DC/DC converter, which is a step-down converter, connects the PV generator and the DC distribution network. Hence, the input voltage v_{pv} should be higher than the output voltage v_s all the time, which is a problem that tends to be overlooked.

During the voltage recovery stage, v_{pv} reaches the minimum value V_{pv}^{min}. Only the condition with $V_{pv}^{min} > V_s^{max}$ can avoid tripping caused by undervoltage faults in practical application. Hence, the value of V_{pv}^{min} should be larger than V_s^{max}, and the influence of parametric effect is worth studying.

Rewriting (3) yields the following equation:

$$C_{pv}\frac{dv_{pv}}{dt} = i_{pv} - v_s \cdot \frac{i_2}{v_{pv}}, \tag{6}$$

where i_{pv} is the output current of the PV panels, and the related parameters are the same as those in **Eq. 3**.

Considering substage II of the voltage recovery phase mentioned earlier, taking the derivation on both sides of **Eq. 5** and combining it with **Eq. 2** yields the following equation:

$$\frac{dP_o}{dt} = v_s\left[k_p\frac{dv_{pv}}{dt} + k_i\left(v_{pv} - v_{pv}^{ref}\right)\right]. \tag{7}$$

Combining **Eqs. 1**–**7** and **Figure 6**, it is found that parameters k_p, k_i, and C_{pv} have a great influence on the dynamic characteristics of the system. Since the system model is a complex non-linear differential equation, it is hard to find symbolic solution. So the numerical solution is adopted, and the phase portrait approach could provide an intuitive analysis.

Figure 7 shows the influences of different parameters. The blue curve represents the relationship between P_{pv} and v_{pv}, while the curves of other colors depict the relationship between P_o and v_{pv} under different conditions. The effects of different k_p with the same k_i and C_{pv} are evaluated in **Figure 7A**, the effects of different k_i with the same k_p and C_{pv} are analyzed in **Figure 7B**, and the effects of different C_{pv} with the same k_p and k_i are depicted in **Figure 7C**.

From the perspective of the system stability, the input PV voltage v_{pv} of the buck DC/DC converter should not be too low. In **Figure 7A**, **Figure 7B**, and **Figure 7C**, V^{min} represents the allowable minimum value of v_{pv} that can ensure normal operation of the DC/DC buck converter. In other words, if the intersection voltage of the two curves lies on the left of V^{min} like point e of the green line in each photo, the breaker will be triggered. As the three pictures show, by increasing k_p, k_i, or C_{pv}, the slope of the $P_o - v_{pv}$ curve will increase, so that the intersection point may move to the right of V^{min}. It is obvious that these parameters have a non-negligible influence on both the dynamic characteristic and transient stability of the whole system.

Substituting (6) and (7) yields the following equation:

$$\frac{dP_o}{dv_{pv}} = v_s\left[k_p + \frac{k_i C_{pv}\left(v_{pv} - v_{pv}^{ref}\right)}{i_{pv} - V_s \cdot \frac{i_2}{v_{pv}}}\right]. \tag{8}$$

Eq. 8 gives the slope of the P_o—v_{pv} curve, which can reflect the variation trend of the P_o—v_{pv} curve.

Proposition 1. During the dynamic process shown in **Figure 6**, the following equation holds:

$$\left(v_{pv} - v_{pv}^{ref}\right)\Big/\left(i_{pv} - v_s \cdot \frac{i_2}{v_{pv}}\right) > 0. \tag{9}$$

Proof. During the dynamic process shown in **Figure 7**, v_{pv} is lower than v_{pv}^{ref} all the time; hence, the numerator is always less than zero. On the other hand, from **Figure 3**, the denominator is

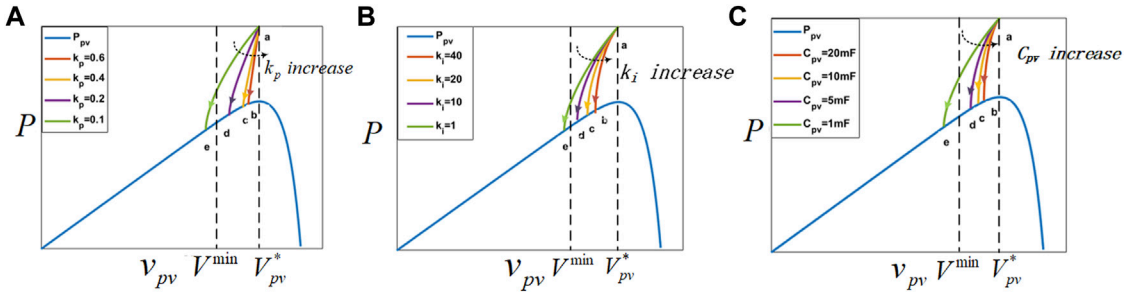

FIGURE 7 | P_{pv}–v_{pv} curve and P_o – v_{pv} curve during the voltage recovery stage. **(A)** k_i = 5, C_{pv} = 1mF, and k_p = 0.1, 0.2, 0.4, and 0.6. **(B)** k_p = 0.1, C_{pv} = 1mF, and k_i = 1, 10, 20, and 40. **(C)** k_p = 0.1, k_i = 5 and C_{pv} = 1mF, 5mF, 10mF, and 20mF.

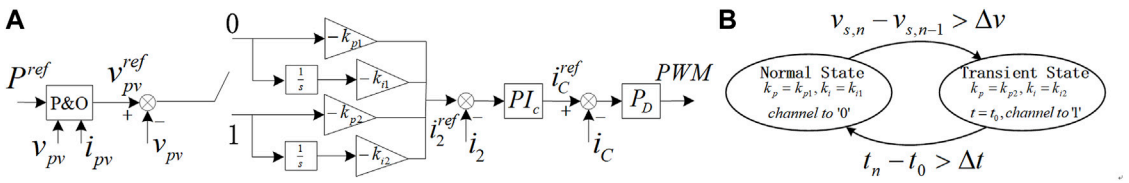

FIGURE 8 | Proposed variable parameter control. **(A)** Control structure. **(B)** Switching logic mode.

essentially the current passing through the capacitor C_{pv}. Then, it is easy to figure out that the denominator is also less than zero as capacitor C_{pv} is discharging. As a result, (9) holds.

Based on Proposition 1, it can be concluded that a larger k_p, k_i, or C_{pv} will cause a larger slope of the P_o—v_{pv} curve, and consequently, the intersection points will be more to the right like from point e to point b, which enhances the transient stability during the voltage recovery stage.

At the same time, from the aforementioned analysis, it can be seen that the stable constraints of small-signal stability and transient stability for controller parameters of PV voltage control loop are mutually contradictory. The proper control parameters can be chosen by making a trade-off between the small-signal stability and the transient stability constraints. The aforementioned conclusions have important value for parameter tuning in the experimental process.

The proposed transient stability analysis method based on the power–voltage evolution curve has many advantages over the existing methods (such as the Lyapunov-based large-signal stability analysis method). First, the Lyapunov method needs to construct an appropriate energy function to analyze the transient stability of the system. The difficulty is that it is not easy to construct the energy function, and the correct result cannot be obtained by using an incorrect energy function. The method proposed in this article does not have this problem, and it is easy to obtain the corresponding relationship between power and voltage, so it is not difficult to analyze the dynamic process of the system in each stage of transient response. Second, the results obtained by using the Lyapunov method are usually conservative, which can only know whether the system is stable but cannot accurately estimate the attraction domain of the system. The proposed method can accurately judge the stability range and stability boundary of the system. Third, the information obtained by using the Lyapunov method is very limited, which is not conducive to revealing the essential stability mechanism of the system. The proposed method can accurately reflect the dynamic response of the system in the transient process and can reveal the stability/instability mechanism of the system well.

VARIABLE PARAMETER CONTROL FOR THE TRANSIENT STABILITY ENHANCEMENT

From the analysis presented in *Transient Stability Analysis Based on the Power–Voltage Evolution Curve* section, the system will lose its stability, and the tripping of circuit breaker may take place when $V^{min}_{pv} < v_s$. In contrast, appropriately increasing parameters k_p, k_i, or $C_{pv}$is beneficial to system stability. Since the capacitor C_{pv} is difficult to be replaced during the actual experiment, it is more common to change the control parameter. Inspired by this mechanism, the variable parameter control is introduced in this section to enhance the system transient stability during the DC bus voltage recovery stage. The basic idea is to increase the values of k_p, k_i appropriately at the beginning of the voltage recovery stage and let them recover after a period of time, which thus guarantees the transient stability during the voltage recovery stage.

Figure 8A shows the proposed variable parameter control structure, and its switching logic is displayed in **Figure 8B**. Compared to the conventional control, as shown in **Figure 1**, only a switching logic mode is added. The subscripts 1 and 2 of

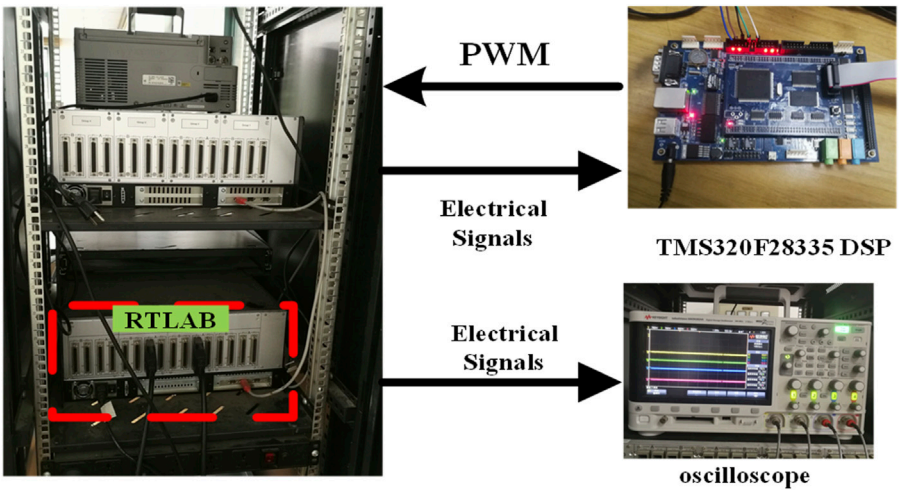

FIGURE 9 | HIL tests setup.

TABLE 1 | Parameters of the system and the PV generator.

Parameter	Value
Filters (L_1, L_2, C)	1.8mH, 1mH, and 30μF
PV capacitance (C_{pv})	1mF
Maximum current (I^{max})	90 A
Reference PV power and voltage (P^{ref}, V^*_{pv})	23 kW, 774 V
Voltage loop (PI)	$k_{p1} = 0.1, k_{i1} = 5$, $k_{p2} = 0.35, k_{i2} = 22.5$
Current loop (PI)	$k_P = 0.01, k_I = 3$
Active damping	$r_c = 0.01$
Voltage change	$\Delta v = 250$V
Time duration	$\Delta t = 0.08$s
Number of modules (N_p, N_s)	13, 30
Short circuit current and open circuit voltage (I_{sc}, V_{oc})	8.21A, 32.9V
Coefficients of current and voltage (K_I, K_V)	0.0032A/K, −0.123V/K
Temperature difference (ΔT)	0
Actual and rated irradiance (G, G_N)	300W/m^2, 1000W/m^2
Thermal voltage (V_t)	1.39V
Ideal diode constant (a)	1.3
Fault detection voltage (Δv)	250 V

the control parameters k_p and k_i represent their values under the normal and transient states, respectively. The two values have the following relationship to ensure that the system gets out of the unstable state as follows:

$$k_{p2} \geq k_{p1}, \tag{10}$$

$$k_{i2} \geq k_{i1}, \tag{11}$$

In the voltage recovery stage, the DC bus voltage increases sharply from V_s^{min} to V_s^{max}. When the voltage sensor detects this step, namely,

$$v_{s,n} - v_{s,n-1} > \Delta v, \tag{12}$$

where $v_{s,n}$ and $v_{s,n-1}$ represent the values of the detected DC bus voltage at the current and last moments, respectively, and Δv is a given voltage value meaning a sudden and significant increase in DC bus voltage. Once this event happens, it suggests that the fault is cleared and the voltage recovery stage begins. The value of k_p and k_i can be appropriately increased to avoid instability.

After a period of time, Δt, k_p, and k_i return to their normal k_{p1} and k_{i1} values. The method to determine Δt is described as follows. In substage IIof the voltage recovery stage, the idea is that before v_{pv} drops to its minimum value V_{pv}^{min}, the value of k_p and k_i remains at their increased values, namely, k_{p2} and k_{i2}, respectively. Considering that the curve of v_{pv} changing with time is smooth, when v_{pv} reaches V_{pv}^{min}, it can be considered that the derivative of v_{pv} with respect to time, namely, dv_{pv}/dt, is equal to zero. Therefore, this time is considered, that is, the time when $dv_{pv}/dt = 0$, minus the time at the beginning of substage II, it is the desired Δt. The main equations have

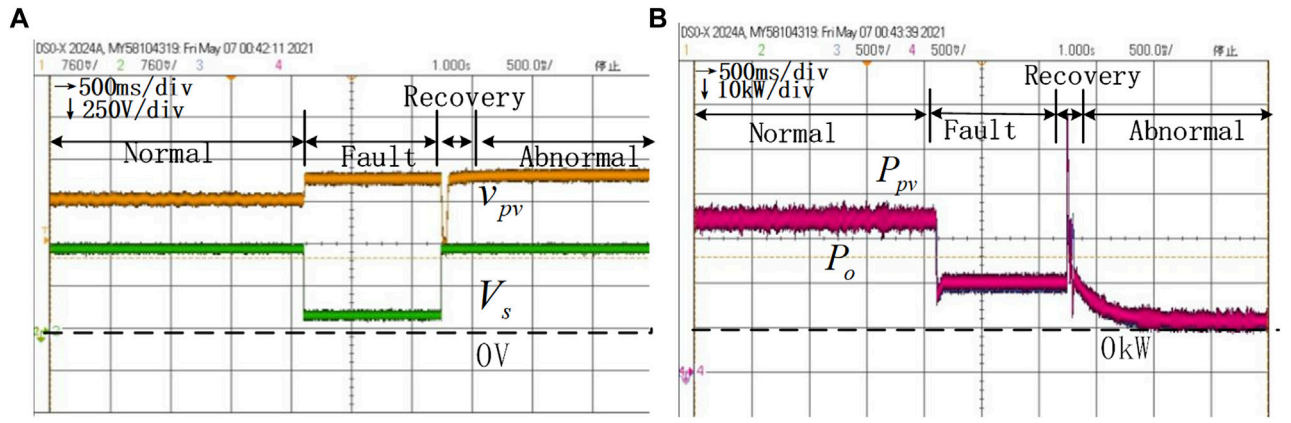

FIGURE 10 | HIL results of voltage dynamics and power dynamics without the variable parameter control under the conditions of k_p = 0.1, k_i = 5, and C_{pv} = 1mF. **(A)** Voltage dynamics of v_s and v_{pv}. **(B)** Power dynamics of P_o and P_{pv}.

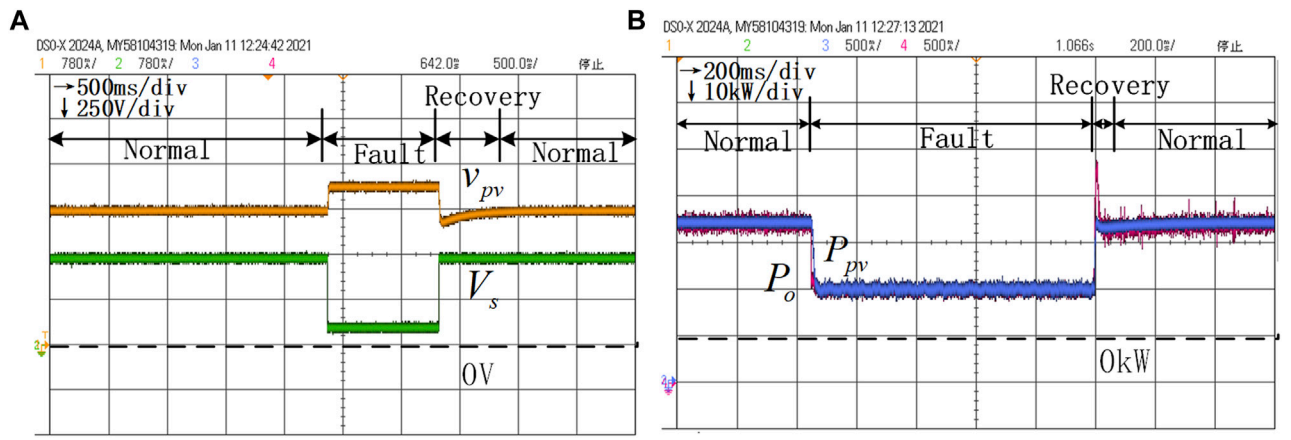

FIGURE 11 | HIL results of voltage dynamics and power dynamics without the variable parameter control under the conditions k_p = 0.6, k_i = 5, and C_{pv} = 1mF. **(A)** Voltage dynamics of v_s and v_{pv}. **(B)** Power dynamics of P_o and P_{pv}.

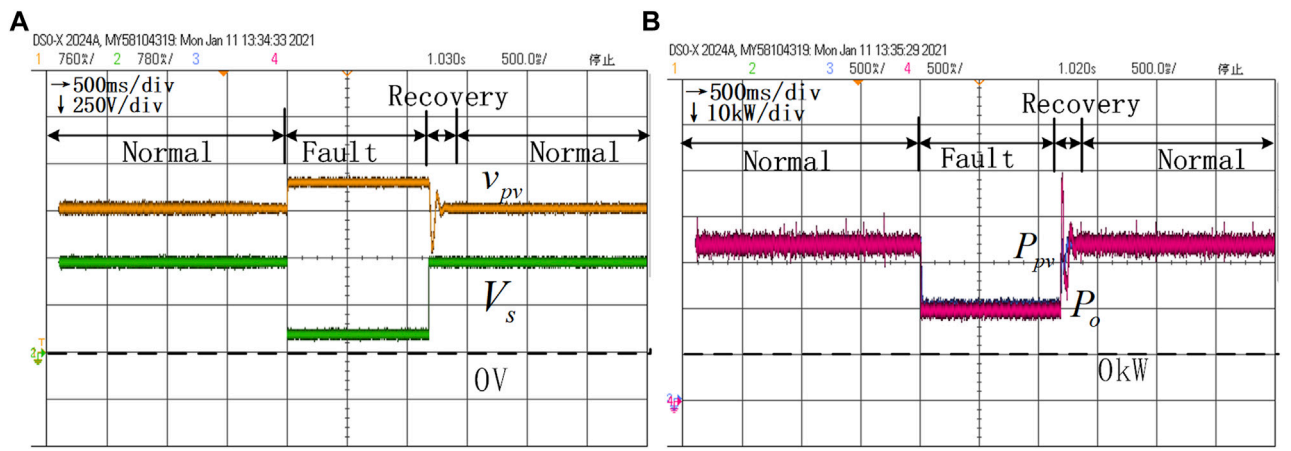

FIGURE 12 | HIL results of voltage dynamics and power dynamics without the variable parameter control under the conditions k_p = 0.1, k_i = 40, and C_{pv} = 1mF. **(A)** Voltage dynamics of v_s and v_{pv}. **(B)** Power dynamics of P_o and P_{pv}.

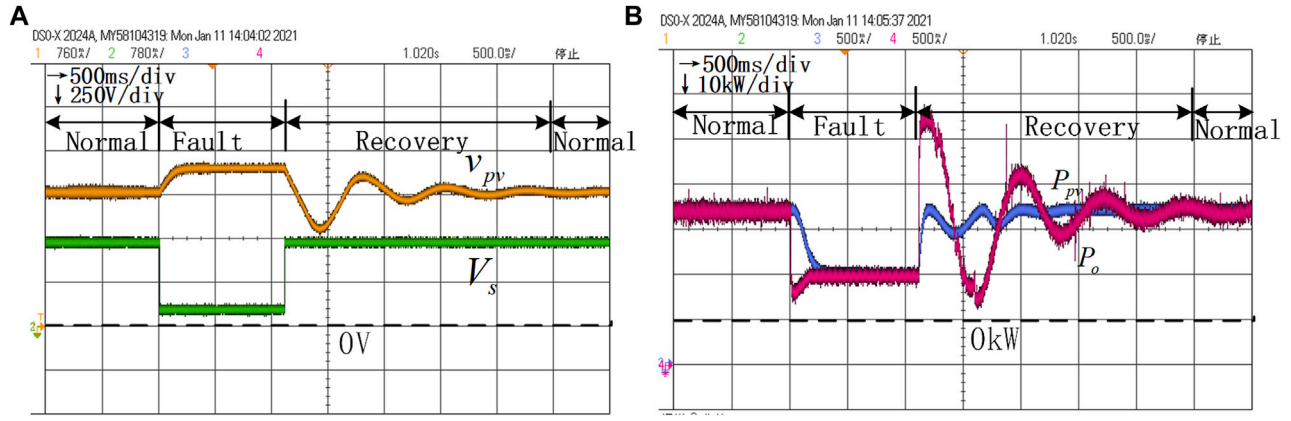

FIGURE 13 | HIL results of voltage dynamics and power dynamics without the variable parameter control under the conditions k_p = 0.1, k_i = 5, and C_{pv} = 20mF. **(A)** Voltage dynamics of v_s and v_{pv}. **(B)** Power dynamics of P_o and P_{pv}.

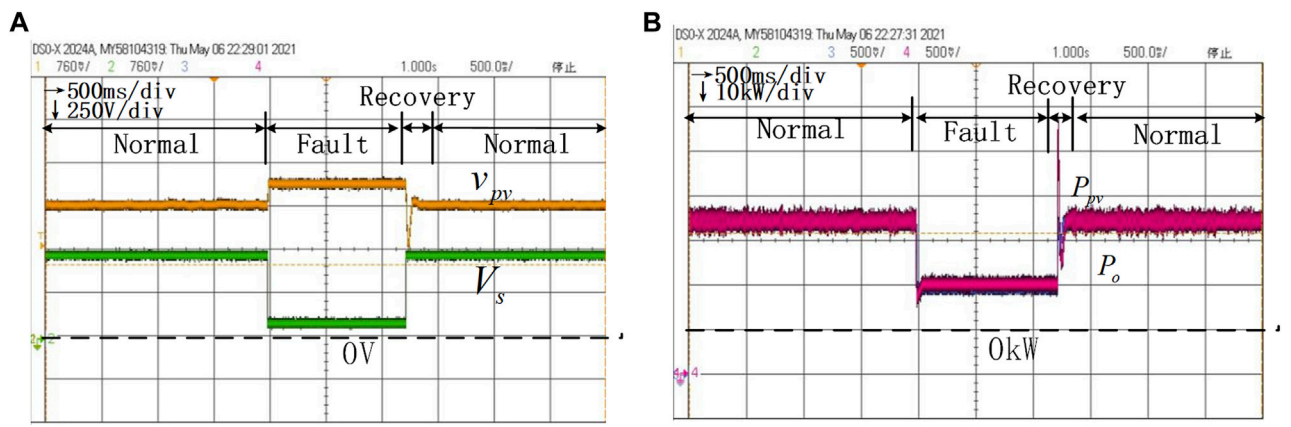

FIGURE 14 | HIL results of voltage dynamics and power dynamics with the variable parameter control under the conditions k_p = 0.1, k_i = 5, and C_{pv} = 1mF. **(A)** Voltage dynamics of v_s and v_{pv}. **(B)** Power dynamics of P_o and P_{pv}.

already been written and now we rewrite them with a few modifications as follows:

$$\begin{cases} \left.\dfrac{dv_{pv}}{dt}\right|_{t=t_3} = \dfrac{1}{C_{pv}}\left(i_{pv} - v_s \cdot \dfrac{i_2}{v_{pv}}\right) = 0 \\ i_{pv} = N_p\left(I_{sc} + K_I \Delta T\right)\left[\dfrac{G}{G_N} - \dfrac{exp\left(\dfrac{v_{pv}}{N_S V_t a}\right) - 1}{exp\left(\dfrac{V_{oc} + K_V \Delta T}{V_t a}\right) - 1}\right], \\ i_2 = I^{max} - k_{p2}\left(V_{pv}^* - v_{pv}\right) - \int_{t_2}^{t_3} k_{i2}\left(V_{pv}^* - v_{pv}\right)dt \\ \Delta t = t_3 - t_2 \end{cases} \quad (13)$$

where t_2 denotes the time when v_{pv} decreases to V_{pv}^* and t_3 denotes the time when v_{pv} decreases to V_{pv}^{min}; the meanings of the other parameters have always been described. Then, Δt can be obtained using (13).

With the power–voltage evolution curve shown in **Figure 6**, the proposed variable parameter control method can increase the slope of the blue curve from point 6 to point 7 by increasing k_p and k_i, which means that the intersection points of two curves will shift to the right. Hence, the value of V_{pv}^{min} will increase and the risk of $V_{pv}^{min} < v_s$ will decrease, thus the stability of the system is enhanced.

HARDWARE-IN-LOOP TESTS

In order to further evaluate the effectiveness of the proposed power–voltage evolution curve analysis and variable parameter control strategy, the corresponding (HIL) experimental tests are conducted using the RT-LAB and TMS320F28335 DSP. The experimental setup of HIL tests is shown in **Figure 9**. The PV generator circuit studied in the experiment, which is identical to that of **Figure 1**, is simulated

in RT-LAB, and the control algorithm is realized using TMS320F28335 DSP.

The whole experiment has experienced four stages: normal stage → fault stage → recovery stage →normal stage. During the normal stage, the DC bus voltage is V_s^{max} = 500V, while in the fault stage, V_s^{min} = 100V. In this test, a voltage drop of more than half of the normal voltage value, that is, 250 V, is considered to enter the fault stage. Hence, the given fault detection voltage Δv = 250V. The other circuit parameters and controller parameters are shown in **Table 1**.

In the following experiments, we test the influence of different parameters and the proposed variable parameter control strategy on the stability of the whole system. These results are shown in **Figure 10**. **Figure 14** contains the voltage and power dynamic processes during the whole process. Fig. (a) of each graph shows the voltage dynamics of v_s and v_{pv}, and Fig. (b) exhibits the power dynamics of P_o and P_{pv}.

Figure 10A and **Figure 10B** show the dynamic process with the initial parameters, that is, k_p = 0.1, k_i = 5, and $C_{pv} = 1mF$. When these parameters are relatively small, it can be seen that v_{pv} drops below v_s, the circuit breaker trips, then the PV output power P_{pv} becomes equal to zero, and v_{pv} becomes the maximum open circuit voltage, indicating that the system cannot return to the normal state and lose stability during the voltage recovery stage in this situation.

Then, increasing the values of different parameters in turn with all other parameters being equal, that is, k_p goes from 0.1 to 0.6 in **Figure 11**, k_i goes from 5 to 40 in **Figure 12**, and C_{pv} goes from 1 mF to 20 mF in **Figure 13**, respectively. From these three pictures, it can be seen obviously that v_{pv} does not decrease below v_s anymore compared with **Figure 10**, and v_{pv} is able to return to its normal value. The experimental results can meet the related analyses well as shown in *Transient Stability Analysis Based on the Power–Voltage Evolution Curve* section B.

Figure 14 shows the voltage dynamics with the proposed variable parameter control under the circumstance of initial parameters, that is, k_p = 0.1, k_i = 5, and C_{pv} = 1mF. The v_{pv} curve is always above the v_s curve which means that the proposed variable parameter control can avoid excessive v_{pv} drop and circuit breaker tripping, then maintain the stability of the system. By comparing **Figure 14** and **Figure 10**, it is easy to see that the system is unstable under the original control method (without the proposed variable parameter control strategy). The stability of the system can be achieved by using the same control parameters after using the proposed variable parameter control strategy, and the superiority of the proposed variable parameter control strategy can be proven. The experimental results verify the effectiveness of the variable parameter control, as shown in *Variable Parameter Control for The Transient Stability Enhancement* section.

It should be noted that in this HIL test, the control parameters, that is, k_p and k_i, are adjusted for only one particular $P_{pv} - v_{pv}$ curve in order to demonstrate the effectiveness of the proposed analysis and control strategy clearly. If environmental parameters such as solar radiation change, the maximum power of PV output will also change. The existing controller parameters also stabilize the system when the $P_{pv} - v_{pv}$ curve changes to a small degree (e.g., the maximum power point voltage V_{pv}^* changes from 774 to 800 V). However, when the $P_{pv} - v_{pv}$ curve changes greatly (e.g., the maximum power point voltage V_{pv}^* changes from 774 to 1600 V), the existing controller parameters often need to be adjusted appropriately. On this basis, other forms of variation can be made. The analysis and control methods proposed in this article can be generalized and applied to other conditions. It is neither necessary nor possible to list all PV curves.

CONCLUSION

This article has analyzed the transient stability of the distributed PV generator connected to the DC distribution network and proposed the variable parameter control method. First, the mathematic model is established when analyzing the transient stability. Then, the transient stability during the DC bus voltage sag and the recovery stage is analyzed using the power–voltage evolution curve. It is shown that the PV side easily suffers undervoltage faults during the transient process, and then the system will lose stability. Moreover, the influence of corresponding control parameters is carefully studied. Next, the variable parameter control is proposed according to the revealed unstable mechanism. Finally, all the findings have been confirmed by hardware-in-loop tests.

DATA AVAILABILITY STATEMENT

The raw data supporting the conclusions of this article will be made available by the authors, without undue reservation.

AUTHOR CONTRIBUTIONS

All authors listed have made a substantial, direct, and intellectual contribution to the work and approved it for publication. The writing of this article was mainly completed by HH, YX and WW provided ideas and guidance for the writing of this article, and PY mainly participated in the experiment.

FUNDING

This work is supported in part by the National Key R&D Program of China (2020YFB1506801), in part by the Science and Technology Project of the State Grid Corporation of China (52110421005H), in part by the National Natural Science Foundation of China (52007162), and in part by the Key R&D Program of Zhejiang Province (2022C01161).

REFERENCES

Azeem, S. W., Chen, W., Tariq, I., Ye, H., and Kaija, D. (2020). A Hybrid Resonant ZVZCS Three-Level Converter Suitable for Photovoltaic Power DC Distribution System. *IEEE Access* 8, 114981–114990. doi:10.1109/access.2020.3002338

Bosco, N., Springer, M., and He, X. (2020). Viscoelastic Material Characterization and Modeling of Photovoltaic Module Packaging Materials for Direct Finite-Element Method Input. *IEEE J. Photovoltaics* 10 (5), 1424–1440. doi:10.1109/jphotov.2020.3005086

Cai, H., Xiang, J., and Wei, W. (2018). Decentralized Coordination Control of Multiple Photovoltaic Sources for DC Bus Voltage Regulating and Power Sharing. *IEEE Trans. Ind. Electron.* 65 (7), 5601–5610. doi:10.1109/tie.2017.2779412

Chaiyatham, T., and Ngamroo, I. (2017). Improvement of Power System Transient Stability by PV Farm with Fuzzy Gain Scheduling of PID Controller. *IEEE Syst. J.* 11 (3), 1684–1691. doi:10.1109/jsyst.2014.2347393

Chen, X., Pei, W., and Tang, X. (2010). "Transient Stability Analyses of Micro-grids with Multiple Distributed Generations," in Proceedings of the 2010 Int. Conf. Power Syst. Technol., Hangzhou, Oct. 2010 (IEEE), 1–8. doi:10.1109/powercon.2010.5666120

Coelho, E. A. A., Cortizo, P. C., and Garcia, P. F. D. (1999). "Small Signal Stability for Single Phase Inverter Connected to Stiff AC System," in Conference Record of the 1999 IEEE Industry Applications Conference. Thirty-Forth IAS Annual Meeting (Cat. No.99CH36370), Phoenix, AZ, USA, Oct. 1999 (Phoenix, AZ, USA: IEEE), 2180–2187. vol.4.

Dahal, S., Mithulananthan, N., and Saha, T. (2011). "An Approach to Control a Photovoltaic Generator to Damp-Frequency Oscillations in an Emerging Distribution System," in Proceedings of the 2011 IEEE Power and Energy Society General Meeting, Detroit, MI, USA, July 2011 (IEEE), 1–8.

Davari, M., and Mohamed, Y. A.-R. I. (2017). Robust Vector Control of a Very Weak-Grid-Connected Voltage-Source Converter Considering the Phase-Locked Loop Dynamics. *IEEE Trans. Power Electron.* 32 (2), 977–994. doi:10.1109/tpel.2016.2546341

Eftekharnejad, S., Vittal, V., Heydt, G. T., Keel, B., and Loehr, J. (2013). Impact of Increased Penetration of Photovoltaic Generation on Power Systems. *IEEE Trans. Power Syst.* 28 (2), 893–901. doi:10.1109/tpwrs.2012.2216294

Eftekharnejad, S., Heydt, G. T., and Vittal, V. (2015). Optimal Generation Dispatch with High Penetration of Photovoltaic Generation. *IEEE Trans. Sustain. Energ.* 6 (3), 1013–1020. doi:10.1109/tste.2014.2327122

Farsi, M., and Liu, J. (2020). Nonlinear Optimal Feedback Control and Stability Analysis of Solar Photovoltaic Systems. *IEEE Trans. Contr. Syst. Technol.* 28 (6), 2104–2119. doi:10.1109/tcst.2019.2929149

Fathabadi, H. (2019). Improving the Power Efficiency of a PV Power Generation System Using a Proposed Electrochemical Heat Engine Embedded in the System. *IEEE Trans. Power Electron.* 34 (9), 8626–8633. doi:10.1109/tpel.2018.2883790

Fu, Q., Nasiri, A., Bhavaraju, V., Solanki, A., Abdallah, T., and Yu, D. C. (2014). Transition Management of Microgrids with High Penetration of Renewable Energy. *IEEE Trans. Smart Grid* 5 (2), 539–549. doi:10.1109/tsg.2013.2286952

Griffo, A., and Jiabin Wang, J. (2012). Large Signal Stability Analysis of 'More Electric' Aircraft Power Systems with Constant Power Loads. *IEEE Trans. Aerosp. Electron. Syst.* 48 (1), 477–489. doi:10.1109/taes.2012.6129649

He, J., Li, Y. W., Bosnjak, D., and Harris, B. (2013). Investigation and Active Damping of Multiple Resonances in a Parallel-Inverter-Based Microgrid. *IEEE Trans. Power Electron.* 28 (1), 234–246. doi:10.1109/tpel.2012.2195032

Hong, L., Shu, W., Wang, J., and Mian, R. (2019). Harmonic Resonance Investigation of a Multi-Inverter Grid-Connected System Using Resonance Modal Analysis. *IEEE Trans. Power Deliv.* 34 (1), 63–72. doi:10.1109/tpwrd.2018.2877966

Huang, Y., Yuan, X., Hu, J., and Zhou, P. (2015). Modeling of VSC Connected to Weak Grid for Stability Analysis of DC-Link Voltage Control. *IEEE J. Emerg. Sel. Top. Power Electron.* 3 (4), 1193–1204. doi:10.1109/jestpe.2015.2423494

Huang, L., Xin, H., Wang, Z., Zhang, L., Wu, K., and Hu, J. (2019). Transient Stability Analysis and Control Design of Droop-Controlled Voltage Source Converters Considering Current Limitation. *IEEE Trans. Smart Grid* 10 (1), 578–591. doi:10.1109/tsg.2017.2749259

Ishchenko, A., Myrzik, J. M. A., and Kling, W. L. (2006). "Transient Stability Analysis of Distribution Network with Dispersed Generation," in Proceedings of the 41st International Universities Power Engineering Conference, Sept. 2006 (Newcastle-upon-Tyne: IEEE), 227–231. doi:10.1109/upec.2006.367749

Jiang, J., Liu, F., Pan, S., Zha, X., Liu, W., Chen, C., et al. (2019). A Conservatism-free Large Signal Stability Analysis Method for DC Microgrid Based on Mixed Potential Theory. *IEEE Trans. Power Electron.* 34 (11), 11342–11351. doi:10.1109/tpel.2019.2897643

Kabalan, M., Singh, P., and Niebur, D. (2017). Large Signal Lyapunov-Based Stability Studies in Microgrids: A Review. *IEEE Trans. Smart Grid* 8 (5), 2287–2295. doi:10.1109/tsg.2016.2521652

Kawabe, K., and Tanaka, K. (2015). Impact of Dynamic Behavior of Photovoltaic Power Generation Systems on Short-Term Voltage Stability. *IEEE Trans. Power Syst.* 30, 3416–3424. doi:10.1109/tpwrs.2015.2390649

Kouki, M., Marinescu, B., and Xavier, F. (2020). Exhaustive Modal Analysis of Large-Scale Interconnected Power Systems with High Power Electronics Penetration. *IEEE Trans. Power Syst.* 35, 2759–2768. doi:10.1109/tpwrs.2020.2969641

Kundur, P. (1994). *Power System Stability and Control*. New York, NY, USA: McGraw-Hill.

Lammert, G., Premm, D., Ospina, L. D. P., Boemer, J. C., Braun, M., and Van Cutsem, T. (2019). Control of Photovoltaic Systems for Enhanced Short-Term Voltage Stability and Recovery. *IEEE Trans. Energ. Convers.* 34 (1), 243–254. doi:10.1109/tec.2018.2875303

Li, H. H. (2013). "Dynamic Modeling of Photovoltaic Grid-Connected System,". M.S. dissertation in *School of Elec. Eng.* (Chongqing, China: Chongqing University). (in Chinese).

Li, N. Y., Liang, J., and Zhao, Y. S. (2011). Research on Dynamic Modeling and Stability of Grid-Connected Photovoltaic Power Station. *Proc. CSEE* 31, 12–18. (in Chinese). doi:10.13334/j.0258-8013.pcsee.2011.10.005

Liu, D. R., Chen, S. R., Ma, M., Wang, H. H., Hou, J. X., and Ma, S. Y. (2011). A Review on Models for Photovoltaic Generation System. *Power Syst. Tech.* 35, 47–52. (in Chinese). doi:10.13335/j.1000-3673.pst.2011.08.017

Majumder, R. (2013). Some Aspects of Stability in Microgrids. *IEEE Trans. Power Syst.* 28 (3), 3243–3252. doi:10.1109/tpwrs.2012.2234146

Priyamvada, I. R. S., and Das, S. (2020). Transient Stability of Vdc - Q Control-Based PV Generator with Voltage Support Connected to Grid Modelled as Synchronous Machine. *IEEE Access* 8, 130354–130366. doi:10.1109/access.2020.3008942

Quan, X., Yu, R., Zhao, X., Lei, Y., Chen, T., Li, C., et al. (2020). Photovoltaic Synchronous Generator: Architecture and Control Strategy for a Grid-Forming PV Energy System. *IEEE J. Emerg. Sel. Top. Power Electron.* 8 (2), 936–948. doi:10.1109/jestpe.2019.2953178

Safayatullah, M., Rezaii, R., Elrais, M. T., and Batarseh, I. (2021). "Review of Control Methods in Grid-Connected PV and Energy Storage System," in Proceeding of the 2021 IEEE Energy Conversion Congress and Exposition (ECCE), Vancouver, BC, Canada, Oct. 2021 (IEEE), 951–958.

Sangwongwanich, A., Yang, Y., and Blaabjerg, F. (2016). High-Performance Constant Power Generation in Grid-Connected PV Systems. *IEEE Trans. Power Electron.* 31 (3), 1822–1825. doi:10.1109/tpel.2015.2465151

Severino, B., and Strunz, K. (2019). Enhancing Transient Stability of DC Microgrid by Enlarging the Region of Attraction through Nonlinear Polynomial Droop Control. *IEEE Trans. Circuits Syst.* 66 (11), 4388–4401. doi:10.1109/tcsi.2019.2924169

Shadmand, M. B., Balog, R. S., and Abu-Rub, H. (2014). Model Predictive Control of PV Sources in a Smart DC Distribution System: Maximum Power Point Tracking and Droop Control. *IEEE Trans. Energ. Convers.* 29 (4), 913–921. doi:10.1109/tec.2014.2362934

Shah, R., Mithulananthan, N., Bansal, R. C., and Ramachandaramurthy, V. K. (2015). A Review of Key Power System Stability Challenges for Large-Scale PV Integration. *Renew. Sustain. Energ. Rev.* 41, 1423–1436. ISSN 1364-0321. doi:10.1016/j.rser.2014.09.027

Song, Q., Zhao, B., Liu, W., and Zeng, R. (2013). An Overview of Research on Smart DC Distribution Power Network. *Proc. CSEE* 33 (25), 9–19. doi:10.13334/j.0258-8013.pcsee.2013.25.009

Sun, J. (2011). Impedance-Based Stability Criterion for Grid-Connected Inverters. *IEEE Trans. Power Electron.* 26 (11), 3075–3078. doi:10.1109/tpel.2011.2136439

Tafti, H. D., Maswood, A. I., Konstantinou, G., Pou, J., and Blaabjerg, F. (2018). A General Constant Power Generation Algorithm for Photovoltaic Systems. *IEEE Trans. Power Electron.* 33 (5), 4088–4101. doi:10.1109/tpel.2017.2724544

Uprety, P., Wang, C., Koirala, P., Sapkota, D. R., Ghimire, K., Junda, M. M., et al. (2018). Optical Hall Effect of PV Device Materials. *IEEE J. Photovoltaics* 8 (6), 1793–1799. doi:10.1109/jphotov.2018.2869540

Villalva, M. G., Gazoli, J. R., and Filho, E. R. (2009). Comprehensive Approach to Modeling and Simulation of Photovoltaic Arrays. *IEEE Trans. Power Electron.* 24 (5), 1198–1208. doi:10.1109/tpel.2009.2013862

Wang, X., and Blaabjerg, F. (2019). Harmonic Stability in Power Electronic-Based Power Systems: Concept, Modeling, and Analysis. *IEEE Trans. Smart Grid* 10 (3), 2858–2870. doi:10.1109/tsg.2018.2812712

Wang, Y., Zhang, L., Li, H., and Liu, J. (2013). Hierarchical Coordinated Control of Wind Turbine-Based DC micro-Grid[J]. *Proc. CSEE* 33 (4), 16–24. doi:10.13334/j.0258-8013.pcsee.2013.04.001

Wang, X., Blaabjerg, F., and Wu, W. (2014). Modeling and Analysis of Harmonic Stability in an AC Power-Electronics-Based Power System. *IEEE Trans. Power Electron.* 29 (12), 6421–6432. doi:10.1109/tpel.2014.2306432

Wang, Y., Silva, V., and Lopez-Botet-Zulueta, M. (2016). Impact of High Penetration of Variable Renewable Generation on Frequency Dynamics in the continental Europe Interconnected System. *IET Renew. Power Generation* 10, 10–16. doi:10.1049/iet-rpg.2015.0141

Weckx, S., Gonzalez, C., and Driesen, J. (2014). Combined Central and Local Active and Reactive Power Control of PV Inverters. *IEEE Trans. Sustain. Energ.* 5 (3), 776–784. doi:10.1109/tste.2014.2300934

Wu, H., and Wang, X. (2020). Design-Oriented Transient Stability Analysis of PLL-Synchronized Voltage-Source Converters. *IEEE Trans. Power Electron.* 35 (4), 3573–3589. doi:10.1109/tpel.2019.2937942

Xia, Y., Yu, M., Wang, X., and Wei, W. (2019). Describing Function Method Based Power Oscillation Analysis of LCL-Filtered Single-Stage PV Generators Connected to Weak Grid. *IEEE Trans. Power Electron.* 34 (9), 8724–8738. doi:10.1109/tpel.2018.2887295

Xiao, Z., and Fang, H. (2010). "Impacts of Motor Load on the Transient Stability of the Microgrid," in Proceedings of the 8th world congress on intelligent control automation, Jinan, China, July 2010 (IEEE), 2623–2627. doi:10.1109/wcica.2010.5554440

Yagami, M., and Tamura, J. (2012). "Impact of High-Penetration Photovoltaic on Synchronous Generator Stability," in Proceeding of the 2012 XXth Int. Conf. Electrical Machines, Marseille, Sept. 2012 (IEEE), 2092–2097.

Zeng, Z., Yang, H., and Zhao, R. (2011). Study on Small Signal Stability of Microgrids: A Review and a New Approach. *Renew. Sustain. Energ. Rev.* 15 (Issue 9), 4818–4828. ISSN 1364-0321. doi:10.1016/j.rser.2011.07.069

Zhang, C., Cai, X., and Li, Z. (2017). Transient Stability Analysis of Wind Turbines with Full-Scale Voltage Source Converter. *Proc. CSEE* 37 (14), 4018–4026.

Zhao, D., Ge, L., Qian, M., Jiang, D., Qu, L., Han, H., et al. (2019). "Review on Modeling of Photovoltaic Power Generation Systems," in Proceeding of the 2019 IEEE Innovative Smart Grid Technologies - Asia (ISGT Asia), Chengdu, China, May 2019 (IEEE), 1943–1946. doi:10.1109/isgt-asia.2019.8881254

Zhou, S., Zou, X., Zhu, D., Tong, L., Zhao, Y., Kang, Y., et al. (2018). An Improved Design of Current Controller for LCL-type Grid-Connected Converter to Reduce Negative Effect of PLL in Weak Grid. *IEEE J. Emerg. Sel. Top. Power Electron.* 6 (2), 648–663. doi:10.1109/jestpe.2017.2780918

Conflict of Interest: The authors declare that the research was conducted in the absence of any commercial or financial relationships that could be construed as a potential conflict of interest.

Publisher's Note: All claims expressed in this article are solely those of the authors and do not necessarily represent those of their affiliated organizations, or those of the publisher, the editors, and the reviewers. Any product that may be evaluated in this article, or claim that may be made by its manufacturer, is not guaranteed or endorsed by the publisher.